Evidence of relationship between strain and In-incorporation: Growth of N-polar In-rich InAlN buffer layer by OMCVD

P. Chauhan,[1,*] S. Hasenöhrl,[1] E. Dobročka,[1] M. P. Chauvat,[2] A. Minj,[2] F. Gucmann,[3] Ľ. Vančo,[4] J. Kováč Jr.,[5] S. Kret,[6] P. Ruterana,[2] M. Kuball,[3] P. Šiffalovič,[7] J. Kuzmík[1]

[1]Institute of Electrical Engineering, Slovak Academy of Sciences, Bratislava, Slovakia

[2]CIMAP, UMR 6252 CNRS, 6 Boulevard Maréchal Juin, 14050 Caen, France

[3]Center for Device Thermography and Reliability, University of Bristol, Bristol BS8 1TL, UK

[4]Slovak U. of Technol., U. Sci. Park Bratislava Centre, Vazovova 5, 812 43 Bratislava, Slovakia

[5]International laser centre, Ilkovičova 3, Bratislava, Slovakia

[6]Institute of Physics, Polish Academy of Sciences, al. Lotników 32/46, 02-668 Warszawa, Poland

[7]Institute of Physics, Slovak Academy of Sciences, Dúbravská cesta 9, 845 11 Bratislava 45, Slovak Republic

*E-mail: prerna.chauhan@savba.sk

ABSTRACT

Two $In_xAl_{1-x}N$ layers were grown simultaneously on different substrates (sapphire (0001) and Ga-polar GaN template) but under the same reactor conditions were employed to investigate the mechanism of strain-driven compositional evolution. The resulting layers on different substrates exhibit different polarities and layer grown on sapphire is N-polar. Moreover, for the two substrates, the difference in degree of relaxation of the grown layers was almost 100%, leading to a large In-molar fraction difference of 0.32. Incorporation of In in $In_xAl_{1-x}N$ layers was found to be significantly influenced by strain imposed by the under-layers. The evolutionary process of In-incorporation during subsequent layer growth along [0001], the direction of growth was investigated in detail by Auger electron spectroscopy. It is discovered that $In_{0.60}Al_{0.40}N$ layer grown directly on sapphire consist of two different regions with different molar fractions: transition and uniform region. According to the detailed cross-sectional transmission electron

microscopy, the transition region is formed near the hetero-interface due to the partial strain release caused by the generation of misfit-dislocations. The magnitude of residual strain in uniform region decides the In-molar fraction. $In_xAl_{1-x}N$ layers were analyzed by structural and optical characterization techniques. Our present work also shows that multi-characterization approach to study $In_xAl_{1-x}N$ is prerequisite for their applications as a buffer layer.

Key words: organometallic chemical vapor deposition, In-rich $In_xAl_{1-x}N$ layer, high-resolution transmission electron microscopy, atomic scanning transmission electron microscopy, Auger electron spectroscopy

INTRODUCTION

As a tunable bandgap (E_g) from the infrared (InN, E_g ~0.7 eV) to the deep ultra-violet (AlN, E_g ~6.2 eV) ternary $In_xAl_{1-x}N$ has a great potential for optoelectronic and electronic devices [1-5]. This further extend to strain engineering by tuning of lattice-parameters from largest InN (a = 3.54 Å, c = 5.76 Å) to smallest AlN (a = 3.11 Å, c = 4.98 Å) either to improve material quality or electronic properties. For example, $In_{0.17}Al_{0.83}N$ lattice matched to GaN, leads to a reduction in the number of defects, and has been using as a barrier layer since last two decades for applications in high electron mobility transistors (HEMTs), light-emitting diodes, laser diodes, solar cells and highly reflective distributed Bragg reflectors [6-10]. In 2011 Kuzmík and Georgakilas [11] have proposed a potential usage of In-rich $In_xAl_{1-x}N$ thick layer as a buffer layer for strained InN-channel HEMTs, which could be promising for high frequency applications.

Growing the high quality $In_xAl_{1-x}N$ layer (either x ~0.17 or x > 0.17) by means of organometallic chemical vapor deposition (OMCVD) technique has always been a

challenge due to the substantial dissimilarities between physical and chemical parameters of binary nitrides, AlN and InN [12, 13]. Growth of $In_xAl_{1-x}N$ alloy over the entire composition range was pioneered by Starosta [14] using reactive multi-target sputtering on microscope glass slides in 1981. Guo et al. [15] has grown $In_xAl_{1-x}N$ in whole composition range directly on (0001) sapphire by reactive radio-frequency magnetron sputtering in 2003. This is probably owing to the fact that sputtering is a physical rather than a chemical deposition technique. Consequently, thermodynamic equilibrium conditions are not required for the growth of $In_xAl_{1-x}N$ layer. Subsequently, number of other techniques have also been reported to grow $In_xAl_{1-x}N$ on conventional GaN buffer layer that include molecular beam epitaxy (MBE) [16-18] and horizontal organometallic chemical vapor deposition (OMCVD) [19-21]. GaN as a buffer layer is an obvious choice for $In_xAl_{1-x}N$ growth because it is used already for high power and high frequency devices. However, parasitic gallium auto-incorporation into $In_xAl_{1-x}N$ layer due to memory effect of GaN base layer growth is another reported issue [22].

To our knowledge, magnetron sputtering has been only reported technique for $In_xAl_{1-x}N$ growth on (0001) sapphire and their optical properties have also been studied [15, 23-25]. Nevertheless, a detailed structural investigation is still missing. In the present work, we compared two $In_xAl_{1-x}N$ layers grown simultaneously under the same growth conditions by OMCVD but on different substrates: (0001) c-plane sapphire and GaN template. We systematically investigated the epitaxial growth conduction by means of high-resolution X-ray diffraction (HR-XRD) method, high-resolution transmission electron microscopy (HRTEM), and scanning transmission electron microscopy (STEM) with atomic resolution. HR-XRD was used to characterize the composition and strain in the $In_xAl_{1-x}N$ layers. In-depth In-composition was analyzed by Auger electron

spectroscopy (AES). Our study of $In_xAl_{1-x}N$ on sapphire provides considerable insight into crystal layer growth, which can be translated onto other rhombohedral substrates as well.

EXPERIMENT

Samples in this study were grown by low pressure OMCVD, using an AIXTRON 3X2″ flip-top (FT) close coupled showerhead (CCS) reactor. Trimethylindium (TMIn), trimethylaluminum (TMAl) and ammonia (NH_3) were utilized as In, Al, and N precursors, respectively. N_2 was used as a carrier gas. The schematic cross-section of two samples is shown in Figure 1 (a, b). The only difference between the samples A and B lies in the under-layers; however the growth conditions for $In_xAl_{1-x}N$ layers were the same. For sample A, $In_xAl_{1-x}N$ was grown directly on sapphire. On the other hand, $In_xAl_{1-x}N$ was grown on GaN template (~2μm GaN grown on sapphire at 1100 °C, then reactor was baked and cleaned prior to the $In_xAl_{1-x}N$ growth) in sample B. For both samples, $In_xAl_{1-x}N$ layers were grown in one run. Prior to the $In_xAl_{1-x}N$ growth initiation, substrates were exposed to NH_3 flow for 300 s at 1011 °C. Following the nitridation, the growth temperature was ramped down to 730 °C in preparation for $In_xAl_{1-x}N$ layer growth. Prior to the $In_xAl_{1-x}N$ layer growth for 8440 s, an AlN layer growth was carried out for 30 s. The other reactor conditions used to grow $In_xAl_{1-x}N$ layers were: $7x10^3$ Pa pressure, 5087 V/III ratio, and 10 slm total gas flow rate. Growth temperature and layer thickness were monitored in-situ using LayTec EpiCurve®TT optical (632.7 nm) reflectance.

HR-XRD measurements were performed using Bruker D8 DISCOVER diffractometer equipped with rotating Cu anode and operating at 12 kW. Diffractions

0004 and $11\bar{2}4$ of $In_xAl_{1-x}N$ were measured to determine molar fraction, lattice parameters, and strain states. A linear dependence of relaxed lattice parameters (a_r, c_r) and elastic coefficients (c_{13}, c_{33}) of $In_xAl_{1-x}N$ on the composition *x* was employed in the calculation. In the evaluation, the values $a_{GaN} = 0.318907$ nm, $c_{GaN} = 0.51855$ nm (PDF 00-50-0792), $a_{AlN} = 0.311117$ nm, $c_{AlN} = 0.498017$ nm (PDF 03–65-0832), and $a_{InN} = 0.35378$ nm, $a_{InN} = 0.57033$ nm (PDF 00-50-1239) were used as initial lattice parameters of GaN, AlN and InN crystals, respectively. The elastic properties of AlN and InN were described by the stiffness constants $c_{13}^{AlN} = 103$ GPa, $c_{33}^{AlN} = 373$ GPa, and $c_{13}^{InN} = 92$ GPa and $c_{33}^{InN} = 224$ GPa, respectively, calculated by density functional-theory [26]. The density of threading dislocations (TDs) in the layers were estimated from the widths (FWHM, β) of the 0002 and $10\bar{1}1$ rocking curves (RCs) measured in symmetric and skew geometry, respectively. ϕ-scans were measured for $10\bar{1}1$ diffraction of $In_xAl_{1-x}N$, and $10\bar{1}4$ and $11\bar{2}3$ diffractions of (0001) sapphire substrate in the range of $0° - 360°$ to assess the orientation relation between $In_xAl_{1-x}N$ lattice and sapphire. Surface morphology of samples was evaluated by using NTEGRA Prima atomic force microscope (AFM) and FEI Quanta 250 FEG scanning electron microscope (SEM). Cross-sectional SEM was also performed to verify the as-grown layers thickness. Elemental depth profile was obtained by Jeol JAMP 9510-F Auger microprobe (using 10 keV electron excitation with 10 nA beam current, 55° tilt and 1 keV Ar^+ ions employed for sputtering) taking advantage of its excellent surface sensitivity and identification of light elements. Due to the lack of standard samples, matrix relative sensitivity factor was not known and correspondingly *y*-axis was calibrated in Auger-peak-to-peak height (APPH) fraction using equal relative sensitivity factors [27]. HRTEM was carried out in an FEI CUBED TITAN microscope equipped with a monochromator and a spherical

aberration (Cs) corrected objective lens. It allows chemical analysis using electron energy loss spectroscopy (EELS) and EDX. The negative Cs mode, which permits to image also light elements, has been used to determine the polarity of the layers in the case of growth on sapphire, which cannot be used as a reference for convergent beam diffraction as it is centro-symmetric. The analysis of the layers crystallographic quality was carried out in the weak beam mode using a JEOL 2010 microscope. Polarized point Raman spectra were measured in $z(xx)\bar{z}$ geometry to observe long-wavelength optical phonon mode behavior by using Renishaw InVia^{TM} Raman spectrometer in confocal mode with 488 nm excitation laser wavelength and ~270 nm spot size on sample. Optical properties were investigated by photoluminescence (PL) and optical absorbance (OA) employing OLYMPUS BX51 microscope equipped with He-Cd laser (325 nm) and Shimadzu UV-VIS-NIR Spectrophotometer SolidSpec-3700, respectively.

RESULTS AND DISCUSSION

The In-incorporation in $In_xAl_{1-x}N$ layer was approximately two times higher when grown on sapphire (In-molar fraction 0.60, sample A) compared to GaN template (In-molar fraction 0.28, sample B). Figure 2 shows a typical 2θ/ω XRD scan of sample A observed in broad range from 30.5 to 36.5°. The full width at half maximum (FWHM) of $In_{0.60}Al_{0.40}N$ 0002 peak observed at 33.07° in 2θ/ω scan is 0.20°. No diffraction peaks are observed at the positions expected for pure InN 0002 at 31.33° and for pure AlN 0002 at 36.14°, which indicates that the obtained 334 nm thick $In_{0.60}Al_{0.40}N$ layer has a single-phase structure and desired growth orientation. The diffraction pattern indicates a heteroepitaxial relationship between $(0001)_{In_{0.60}Al_{0.40}N}$ and $(0001)_{Al_2O_3}$. The rocking curve (ω-scan) of $In_{0.60}Al_{0.40}N$ 0002 and $10\bar{1}1$ diffractions has a FWHM value of 0.20°

and 0.77°, respectively. The corresponding screw and edge dislocation densities calculated according to [27, 28] are 2×10^9 cm^{-2} and 1×10^{11} cm^{-2}, respectively. This indicates that $In_{0.60}Al_{0.40}N$ layer reported here has better quality than other published MBE grown layers of same In-molar fraction with FWHM of 0.51° [18] and 0.67° [29] measured by ω-scan of 0002 diffraction.

In the case of sample A, the degree of in-plane alignment of $In_{0.60}Al_{0.40}N$ relative to the (0001) Al_2O_3 substrate was determined by evaluation of ϕ-scans as given in Figure 3. Three ϕ-scans, $10\bar{1}4$ and $11\bar{2}3$ of the (0001) Al_2O_3 substrate and $10\bar{1}1$ of $In_{0.60}Al_{0.40}N$ layer were measured in the whole 360° range of the azimuthal angle. Note the threefold symmetry of the $10\bar{1}4$ scan that reflects the rhombohedral symmetry of the Al_2O_3 lattice. It is seen that the positions of the $10\bar{1}1$ maxima perfectly coincide with the maxima of $11\bar{2}3$ scan of the substrate indicating that the in-plane direction $[10\bar{1}0]$ of $In_{0.60}Al_{0.40}N$ is parallel with the direction $[11\bar{2}0]$ of Al_2O_3. That means the $In_{0.60}Al_{0.40}N$ lattice is 30° rotated with respect to Al_2O_3, which is the same rotation as observed for GaN on Al_2O_3 [30] and hence, the same applies to sample B. One can summarize the in-plane heteroepitaxial relationship between $In_xAl_{1-x}N$ grown on Al_2O_3 as $In_xAl_{1-x}N(0001)[10\bar{1}0] \| Al_2O_3(0001)[11\bar{2}0]$ and we assume that this relationship holds for the whole composition range of $In_xAl_{1-x}N$. Schematic representation of the interface between the (0001) Al_2O_3 substrate and the InAlN layer is shown in Figure 3(b).

The designed samples A and B exhibit a large strain difference in $In_xAl_{1-x}N$ layers as a consequence of using different under-layers. The precise values of *x* were calculated from the positions of 0004 and $11\bar{2}4$ diffractions in reciprocal space determined by HR-XRD. Hexagonal c-oriented epitaxial layers are transversely isotropic, i. e. the deformation of the layer is completely described by two non-zero strain components:

$$\varepsilon_{\parallel}(x) = \frac{a - a_r(x)}{a_r(x)}, \varepsilon_{\perp}(x) = \frac{c - c_r(x)}{c_r(x)}, \quad (1)$$

where a, c and a_r, c_r are the lattice parameters of strained (and measured) and fully relaxed layer, respectively. These components are connected by the relation

$$\varepsilon_{\perp} = -2\frac{c_{13}(x)}{c_{33}(x)}\varepsilon_{\parallel}. \quad (2)$$

It has to be pointed out that in addition to the relaxed lattice parameters a_r, c_r, the aspect ratio c_r/a_r as well as the elastic properties expressed by c_{13}/c_{33} are functions of the composition x as indicated above. Therefore the equations (1) and (2) for unknown values of a_r, c_r, $\varepsilon_{\parallel}$ and x have to be solved numerically. An efficient and simple iterative procedure for this solution was proposed in Chauhan et al. [27]. It was also shown that for ternary compounds the solution is unique for the given input parameters a and c determined experimentally. Using this procedure, the layer composition x for samples A and B was precisely determined taking correctly into account the in-plane strain component $\varepsilon_{\parallel}$. For the measured and calculated in-plane lattice parameters a and a_r the degree of relaxation R is standardly evaluated as

$$R = \frac{a - a_{sub}}{a_r - a_{sub}}, \quad (3)$$

where a_{sub} is the in-plane lattice parameter of the substrate.

For sample A the values $\varepsilon_{\parallel} \sim 0$ and $R \sim 1$ were obtained, i. e. the layer is completely relaxed. In the case of sample B, however, the strain in $In_xAl_{1-x}N$ layer is –1.4% and $R \sim 0$, which means the strain in the $In_xAl_{1-x}N$ layer is compressive and is almost completely preserved. Considering that $In_xAl_{1-x}N$ layers in sample A and B were grown under the same growth conditions, it is reasonable to assume that a large In-molar fraction

difference strongly depends on the kind of the substrate used in the experiment and is closely connected with the residual strain in the layer.

Unlike on polar substrates (SiC), the polar orientation is not obvious in the case when layer grown on non-polar substrates (Al_2O_3). In this study, the polarity of samples was determined by two techniques: CBED and negative Cs HRTEM. The high resolution analysis with negative Cs has been especially carried out on sample A to determine the polarity, which cannot be determined by convergent beam electron diffraction, because the layer contains a high density of defects. On the other hand for sample B, the polarity is determined by convergent beam diffraction on the GaN template and InAlN followed the same polarity. Under the growth conditions described in experimental section, we obtained $In_xAl_{1-x}N$ layers of both types of polarities. N-polar $In_xAl_{1-x}N$ layer was obtained for the layer grown on nitridated Al_2O_3 for 300 s at 1011 °C. However, $In_xAl_{1-x}N$ layer of sample B, grown on GaN template was In/Al-polar. A HRTEM image of N-polar $In_xAl_{1-x}N$ layer of sample A is displayed in Figure 4, this negative Cs image shows the bond orientation, and clearly demonstrates the N-polarity. The observed influence of long and high temperature nitridation and of hetero-interface on $In_xAl_{1-x}N$ layer polarity is consistent with the earlier reported investigations, and detailed explanation can be found elsewhere [31-33].

The high vapor pressure and following low growth efficiency of nitrogen (N) could lead to the formation of InN–In_2O_3 alloy and resulting bandgap discrepancies have been reported for InN. In order to track the In, N, Al, oxygen (O) and carbon (C) profiles of samples A and B along [0001] direction, AES depth profile was measured and the typical AES profiles are shown in Figure 5. Due to a mixing of atoms sputtered from very thin AlN layer with the atoms originating from adjacent layers at the high sputtering rates

during AES depth profiling, the 1-2 nm thick AlN layer, as shown in Figure 1, is not visible in AES profiles of samples. Evidently, $In_xAl_{1-x}N$ layer of sample A consists of two different regions with different molar fractions: a transition region (light blue region) and a uniform region. In the transition region, In- and Al-molar fractions vary, while they remain nearly the same in the uniform region. For sample A, the Al-molar fraction falls and the complimentary In-molar fraction rises rapidly in the initial stage of growth, which corresponds to 50 nm thick transition region (at the depth ≥275 nm). With the progression of growth, the In-molar fraction enters into the uniform region with In-molar fraction of 0.60. The transition region occupies a comparatively small part in $In_xAl_{1-x}N$ layers, therefore, the residual strain determined by HR-XRD can be approximately equivalent to the residual strain in the uniform region. The observed decreasing profile of oxygen in the transition region along the growth direction could be attributed to its out-diffusion from sapphire [34, 35]. Carbon content close to surface is mainly due to environmental contamination. AES observations indicate that the layer grown on sapphire is homogeneous, considering the measured in-depth distribution of the elements, and has insignificant amount of oxygen impurity.

In the case of sample B, $In_xAl_{1-x}N$ layer growth mechanism seems to be additionally complicated due to the existing Ga profile in the transition regions, which could be out-diffused from the underlying GaN layer [22, 36]. We did not observe unwanted Ga in $In_xAl_{1-x}N$ layer of sample A that ruled out growth environment and lingering precursors for being the source of Ga in the transition region of sample B [37]. It is found that In and Al-incorporation in 40 nm thick transition region is complementary to the diminishing Ga profile in the subsequent layer growth. On the contrary to sample A, no uniform region is observed in sample B. This could be attributed to the 17 nm RMS

surface roughness of the layer that may influence depth resolution and leads to the increasing interface widening with sputtered depth. With the progression of growth, we observe gradual and slow increase of In-incorporation. Quantitatively, for $In_xAl_{1-x}N$ layers of samples A and B, the large difference of degree of relaxation close to 100% could leads to a large In-molar fraction difference of 0.32 in the uniform region. The compressively strained layer on GaN template results with a 0.28 In-molar fraction, which is close to the previous studies on $In_xAl_{1-x}N$ [38] and $In_xGa_{1-x}N$ [39] under certain growth conditions. These phenomena can be elucidated by compositional pulling effect (CPE) guided by compressive strain [40].

The observed different thicknesses or growth rates of $In_xAl_{1-x}N$ layers of samples A (~0.04 nm/s) and B (~0.02 nm/s), indicate that not only In-incorporation, but also that the growth rate is influenced by different under-lying substrates. The approximately two times higher growth rate and In-molar fraction of $In_xAl_{1-x}N$ layer of sample A compared to sample B indicate that In-incorporation efficiency depends on growth rate, which is consistent with the previous reports on $In_xGa_{1-x}N$ [41] and $In_xAl_{1-x}N$ [42] as well. Typically, the high defect density in a layer arise from the large residual in-plane strain that is generated by the large lattice mismatch to the used substrate (will be discussed in TEM section) and consequently, relaxed $In_xAl_{1-x}N$ layer of sample A could provide a favorable accommodation to the larger size of In adatoms. According to Keller et al. [43], polarity of layers influence In-incorporation as well. Whereas in our previous reports [27, 44], we observed that strain relaxation is accompanied by enhanced In-incorporation on In/Al-polar InAl(Ga)N/GaN layers. Therefore, the extent of effectiveness of polarity still need to be demonstrated. In the following, we will focus exclusively on the experimental

analysis of In-rich $In_xAl_{1-x}N$ layer grown directly on sapphire (sample A), which is the sample of our interest.

Cross sectional TEM analysis was performed to analyze the growth evolution of $In_xAl_{1-x}N$ on sapphire, and subsequently identify dislocations and the possible origin of surface defects. Figure 6 shows a weak beam dark field image recorded with **g** = 0002, where the interface and the surface of the layer are seen edge-on. In this figure, the following important features can be noticed: First, on the top of sapphire substrate a slightly bright contrast is visible in the $In_xAl_{1-x}N$ layer with an extension of around 40 nm, which means that there is a high density of defects. It is worth mentioning here that 1-2 nm AlN layer could be too thin to have an effect on strain, nevertheless, promote strain relaxation in uncovered areas. On top of this area, the individual threading dislocations with **c** component are clearly visible and they propagate to the layer surface. Some of them can be seen to induce visible change at the layer surface probably through the formation of pinholes. Finally, the layer surface is not completely flat even at this scale. With an estimate of an average thickness of ~100 nm, there are visible 36 dislocations in this image, which gives a density of around $2.6x10^{10}$ cm^{-2}.

The picture is more complex in weak beam images recorded using **g** = $10\bar{1}0$ (figures 7) where the bright contrast at the $In_xAl_{1-x}N$/Sapphire interface is increased. This is a clear indication that this interface area contains the highest density of defects especially with displacement vectors (Burgers Vectors) inside the basal planes. Such defects may be **a** and **a+c** as well as stacking faults [45]. Specifically, the stacking faults are not visble when using **g**= 0002, or **g**= $11\bar{2}0$ which agrees with the lower contrast exhibited in the interfacial area in the corresponding images. Such stacking faults would

be easily identified using high resolution transmission electron microscopy as has been reported earlier [46, 47].

On top of the nucleation layer, it becomes difficult to determine the density of the threading dislocations, which is much higher than in figure 6 and majority of dislocations are of **a** type. A close examination of the figure shows that there are many bright bands extended from the top of the interface to the surface. These areas correspond to the walls of **a** threading dislocations, which are so close that cannot be separated in this mode of imaging [48]. The micrograph recorded with $\mathbf{g} = 11\bar{2}0$ is shown in figure 8 and also presented the contrast at the interface but with a lower density, which is a strong indication of the presence of stacking faults close to the interface. Bright bands of closely spaced **a** type threading dislocations are also clearly exhibited, and the density of these dislocations is extremely high with lines possible to distinguish towards the layer surface.

The relaxation of the misfit strain has been investigated for the growth of the wurtzite GaN buffer layer on sapphire, theoretically [49] as well as experimentally by OMCVD [50] and MBE epitaxy [51]. In the case of conventional buffer GaN on sapphire, the 16% lattice mismatch has been shown to relax rapidly, mainly inside the buffer layer through the formation of multiple types of extended crystallographic defects including basal [50] and prismatic stacking faults [47], but also a strong probability of inversion domains formation [52, 53]. Such high defect densities are mainly confined very close to the interface and with a fast decrease of the defect density up to 6-7 $x10^8$ cm^{-2} at layer thicknesses of around 0.5 µm [52]. In this report, with 22% lattice mismatch on sapphire, $In_{0.60}Al_{0.40}N$ layer is expected to becomes relaxed very quickly (the theoretical critical thickness is ~0.76 nm) which should be expected to lead to the localization of most of the strain very close to the interface. However, the density of extended defects inside the

epitaxial layer is extremely high, probably in the range of 10^{11} cm^{-2} as seen above. The detailed investigation of this growth evolution is still underway and will be reported separately [54].

To investigate the influence of different substates on surface morphology $In_xAl_{1-x}N$ layers were analyzed by AFM and SEM measurements. Figure 9 presents the AFM and SEM images of the surface of $In_xAl_{1-x}N$ layer grown on sapphire. $In_xAl_{1-x}N$ layer exhibits grain-like surface morphology with flat tops that wrap around dislocations, which is a characteristic of 2D step-flow (step height ≥ 2 MLs) growth mode on top of 3D islands. The observed surface morphology is identical to that of InN grown by MBE [55, 56]; being induced by long and high-temperature nitridation and is usually attributed to N-polar layers [31]. The root-mean-square (RMS) surface roughness is ~1 nm over the scan area of 1x1 μm^2, which is lower than previously reported by Guo et al. [15, 23]. However, RMS roughness of $In_xAl_{1-x}N$ layer grown on GaN template is ~17 nm. It is thus proposed that the growth mechanism is changed in $In_xAl_{1-x}N$ layer grown directly on sapphire because of different surface kinetics.

The quantitative analysis was performed using SPM data visualization and analysis tool Gwyddion [57]. From the topography, an average pinhole density of 2.6 (±1.48) x10^9 cm^{-2} and an average RMS roughness of 5.95±1.4 nm were estimated over 2.5x2.5 μm^2 scanned area. Besides low-roughness granular morphology, distinct planar grains with relatively increased height of 20-24 nm (area) and dislocations decorated at their boundaries are observed. Over a scan area of 12x12 μm^2, these grains account for ~25% of the total area with the grain mean height ~20±1 nm for 44% of grain population and 20-30 nm of the rest. Surface diameter of the grains varies between 200 and 500 nm for 80%. These characteristics show some similarities with the schematic

growth of the GaN epilayer which has been described previously to understand the presence of edge-type threading dislocations at the coalesced grain boundaries of nano-islands with small twist angles [58]. From the TEM and X-ray rocking curves analysis, this is confirmed that most of the dislocations are of edge-type. Finally, since the surface can be described as granular, the numerically calculated height-height correlation function (HHCF) can be employed for quantitative estimation of surface roughness and lateral correlation length (Figure 10). The HHCF can be described using a Gaussian distribution defined as

$$\mathrm{HHCF(X)} = 2\sigma^2[1 - \exp(-\mathrm{X}^2/\lambda^2)] \quad (4)$$

where σ and λ are RMS roughness and lateral correlation length, respectively. This analysis was applied over an area of 30x30 μm^2, and from the fitting of the correlation function, the parameters σ = 5.66 nm and λ = 223.60 nm were extracted. The roughness extracted is of similar magnitude as roughness calculated conventional way. The correlation length would roughly correspond here to the average grain size.

To validate the inherent optical properties of the as-grown $In_xAl_{1-x}N$ layer on sapphire, the absorption edge (AE) energy of the sample was determined by extrapolating the almost linear portion of the optical-absorbance spectrum, as presented in Figure 11. Non-parabolic conduction band could be the probable reason behind the non-linear absorbance plot [18]. The estimated value of 1.68 eV for the intrinsic bandgap energy of $In_{0.60}Al_{0.40}N$ layer is consistent with the bandgap of layers fabricated by MBE [18] and OMCVD [59]. However, lower than the layers (~2.8 eV) grown by reactive RF magnetron sputtering [15, 23] and RF-MBE [29], which are close to the theoretical bandgap ~2.88 eV estimated by using Vegard's law. It is worth mentioning that layer bandgap remains unaffected by the presence of negligible amount of oxygen impurity as

demonstrated in Figure 5 (a). OA spectrum is complemented by a sharp, symmetric PL emission peak of $In_{0.60}Al_{0.40}N$ located at 1.79 eV (FWHM = 0.20 eV) as shown in Figure 11. An insignificant amount of Stokes shift of ~0.11 eV is observed that is, however, lower than the width of PL peak. We assume that this disagreement could be because of random local fluctuations of locally alloyed layer. The deviation from Vegard's law could be defined by the bowing parameter b = 4.53 (for PL) and b = 5.15 (for OA) after using 0.7 eV InN bandgap and 6.14 eV AlN bandgap.

To complete the structural characterization of $In_xAl_{1-x}N$ layer grown directly on sapphire, which is a less studied system and likewise experimental Raman scattering data, we performed Raman spectroscopy. In Raman spectrum, single-mode behavior of E_2(high) phonon (529 cm^{-1}), and dual-mode behavior of A_1(LO) phonon, InN-like (650 cm^{-1}) and AlN-like (726 cm^{-1}), are observed for sample A as displayed in Figure 12. The observed two-mode behavior of the A_1(LO) phonon in In-rich $In_{0.60}Al_{0.40}N$ layer agrees well with the works of Kang et al. [20, 60] and Tangi el al. [61]. After using the linear relation between phonon frequency and composition as reported by Kang et al. [20, 60] as a reference, we conclude that the E_2(high) (FWHM = 58 cm^{-1}) is red-shifted by 8 cm^{-1}. On the other hand, InN-like (FWHM = 121 cm^{-1}) and AlN-like A_1(LO) (FWHM = 63 cm^{-1}) phonon frequencies are blue-shifted by 13 and 4 cm^{-1}, respectively. According to the theoretical and experimental investigations of Davydov et al. [62] and Bergman et al. [63], the phonon energies depend on Al-molar fraction in $Al_xGa_{1-x}N$ and shift towards higher frequencies with increasing Al-molar fraction. This further leads to the phonon line broadening due to elastic scattering of phonons by fluctuations in randomly disordered composition. Phonon frequency shift could also be attributed to the phonon frequency dependence on free carrier concentration and electric field [64, 65].

Olive et al. [66] observed a bowing in E_2(high) frequency relationship with In-molar fraction in $In_xGa_{1-x}N$ and showed that frequency of A_1(LO) phonon mode is strongly influenced by in-depth composition gradients/strain. In the present work, we conclude that the measured red-shifted E_2(high) frequency of In-rich $In_{0.60}Al_{0.40}N$ layer exhibits a single-mode behavior and suffers from the bowing effect. Furthermore, we conclude that the measured A_1(LO) frequency of In-rich $In_{0.60}Al_{0.40}N$ layer exhibits two-mode behavior; InN-like A_1(LO) frequency is blue-shifted when compared to AlN-like A_1(LO) due to the In-rich layer and consequently, more broadened due to elastic scattering of phonons by the random disordered compositional fluctuations. The extent of compositional fluctuations in this sample is still under study and will be reported elsewhere [54]. Further research on the role of the $In_xAl_{1-x}N$ buffer layer is needed to investigation electrical properties.

CONCLUSION

We provide an experimental evidence of correlation between In-incorporation and strain in the N-polar $In_xAl_{1-x}N$ layer that can promote growth of thick In-rich $In_xAl_{1-x}N$ layer applicable to a variety of promising application or more specifically, as a buffer in InN channel transistor for THz applications. The different substrates, sapphire and GaN template, strongly affect the strain-relaxation mechanism of $In_xAl_{1-x}N$ layers resulting in an increase of the In-molar fraction from 0.28 for GaN template to 0.60 for sapphire, and growth rate from ~0.02 nm/s to ~0.04 nm/s, respectively. $In_xAl_{1-x}N$ layer on sapphire was fully relaxed. On the contrary, the $In_xAl_{1-x}N$ layer grown on GaN template was completely compressively strained. For $In_{0.60}Al_{0.40}N$ layer we observed optical bandgap variation from 1.68 to 1.79 eV, as measured by OA and PL, respectively. In-rich

$In_{0.60}Al_{0.40}N$ layer also demonstrated single-mode behavior of E_2(high) phonon, and dual-mode behavior of A_1(LO) phonon, InN-like and AlN-like. Along with the above mentioned characterizations that confirmed a good quality of 334 nm thick N-polar $In_xAl_{1-x}N$ polycrystalline layer grown on sapphire, we proposed a novel approach to grow In-rich $In_xAl_{1-x}N$.

ACKNOWLEDGEMENTS

The authors would like to acknowledge the financial support granted by the Slovak Agency for R&D: project no. APVV-15-0031 and APVV SK-CN-RD-18-0006.

Figure Caption

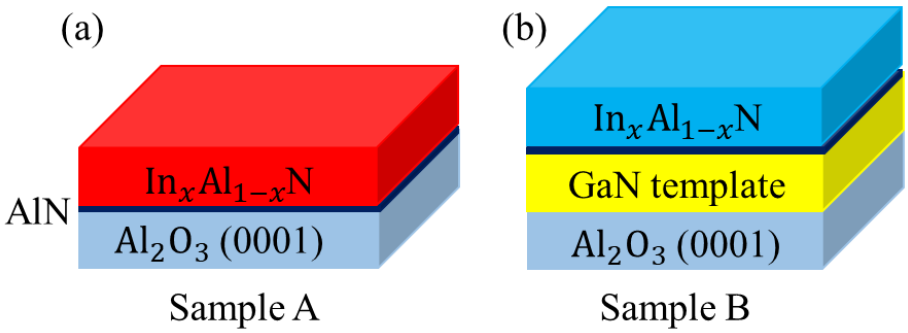

Figure 1. (a) Schematic layer structure illustration for sample A. The deposition was initiated with nitridation, followed by a 1-2 nm-thick HT-AlN nucleation layer and 334 nm-thick $In_xAl_{1-x}N$ layer. (b) Schematic layer structure illustration for sample B. The layer structure consists of a ~2μm-thick GaN template grown on Al_2O_3 (0001), and $In_xAl_{1-x}N$ layer.

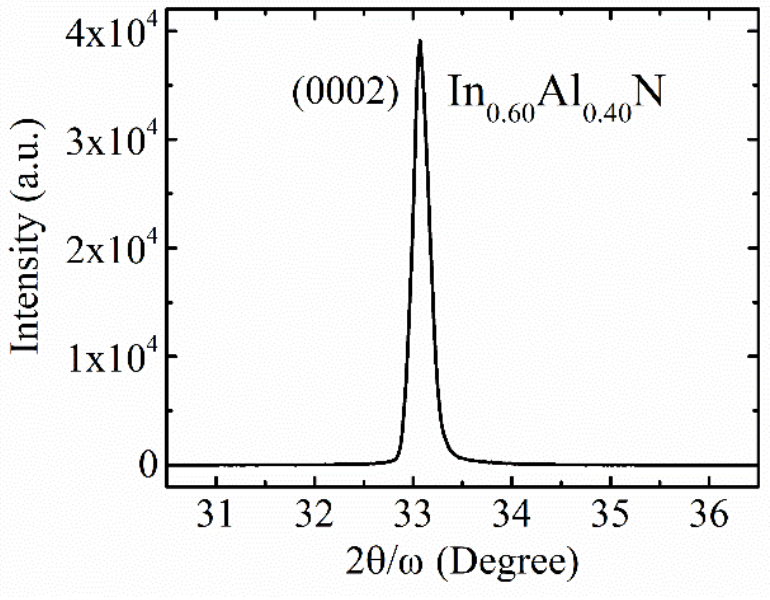

Figure 2. Representative XRD 2θ/ω scan of $In_{0.60}Al_{0.40}N$ grown on (0001) sapphire.

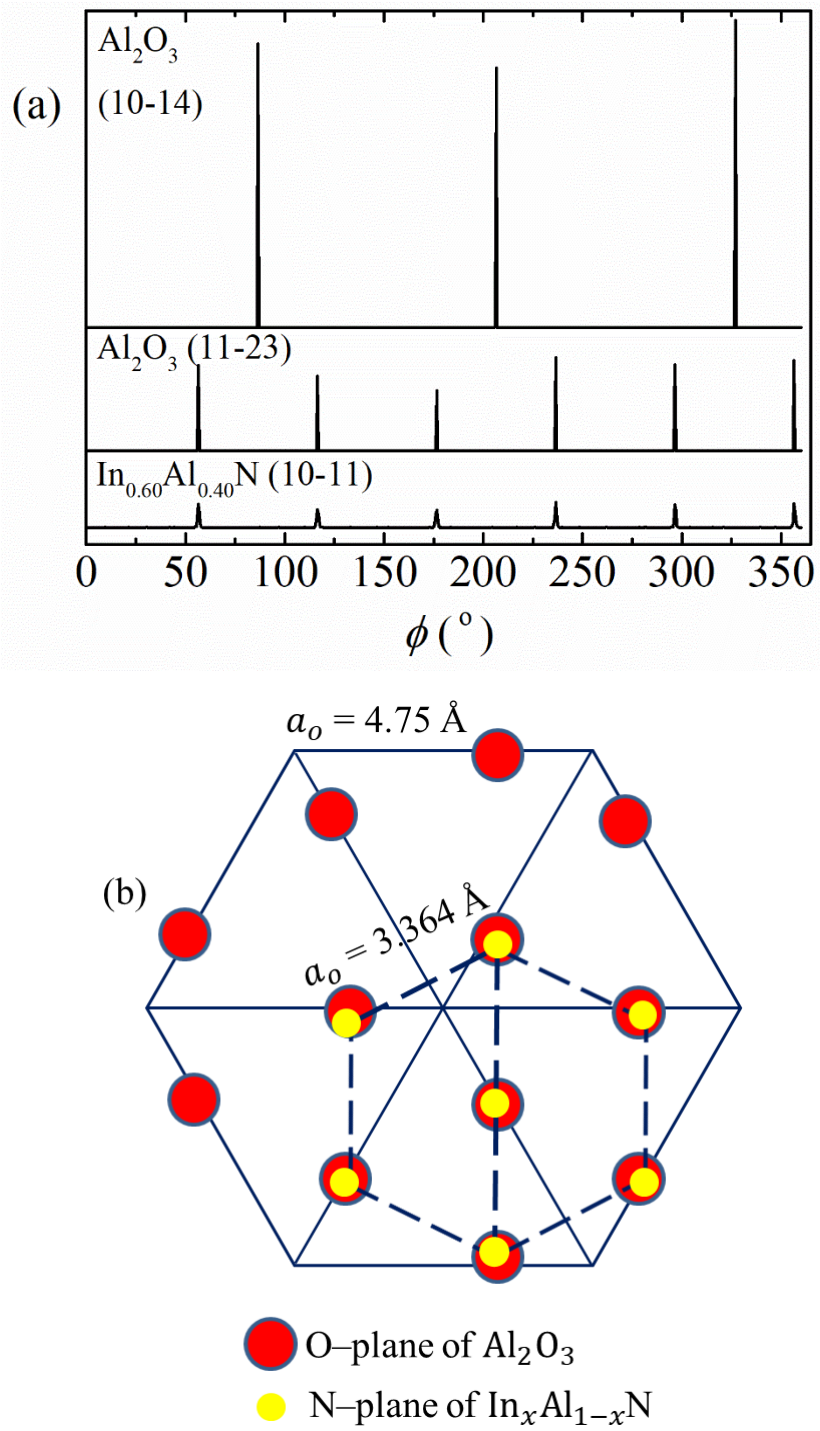

Figure 3. (a) XRD ϕ-scans of $10\bar{1}4$, $11\bar{2}3$ diffraction of (0001) Al_2O_3 substrate and $10\bar{1}1$ diffraction of grown $In_{0.60}Al_{0.40}N$ layer. (b) Schematic drawing of epitaxial matching relation between Al_2O_3 and $In_xAl_{1-x}N$ at interface.

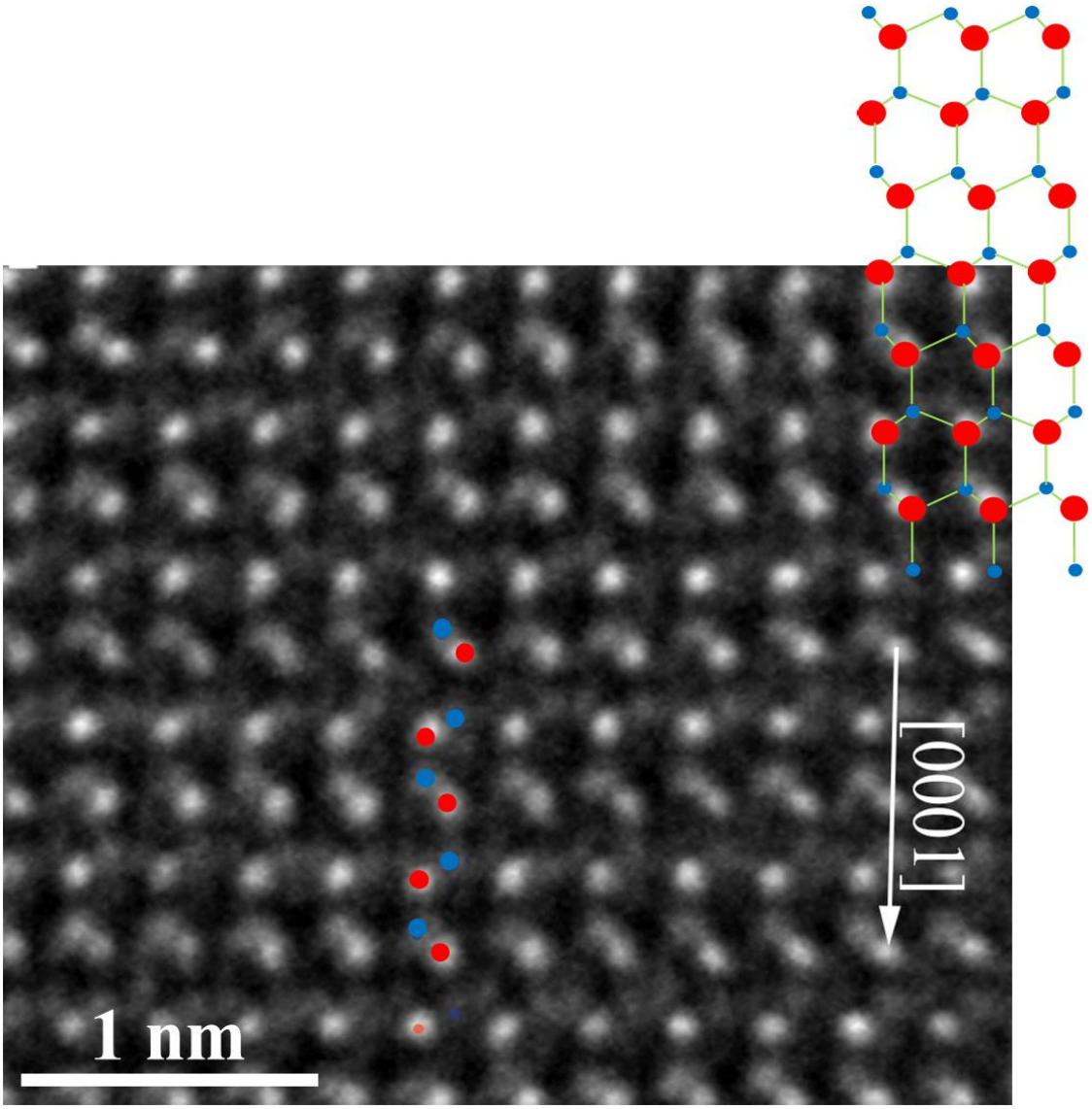

Figure 4. Negative Cs HRTEM image of $In_xAl_{1-x}N$ layer of sample A showing aligned columns of N atoms (blue) and In/Al atoms (red). The layer is N-polar, for this image, the Cs was set to -40 µm.

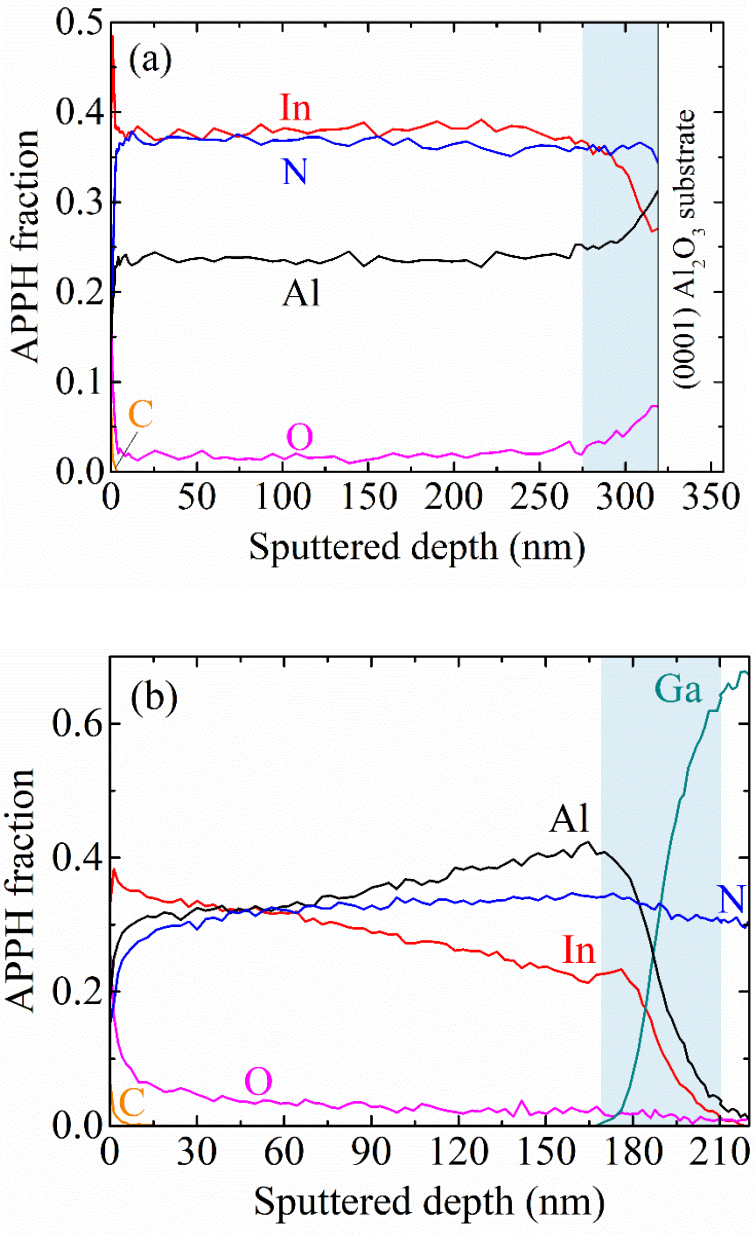

Figure 5. In, N, Al, O and C elemental depth profiles in $In_xAl_{1-x}N$ layers along the growth direction [0001] for (a) sample A and (b) sample B. Thickness of $In_xAl_{1-x}N$ layers of sample A and B is approximately 334 nm and 210 nm, respectively. The light blue area is corresponding to the transition region.

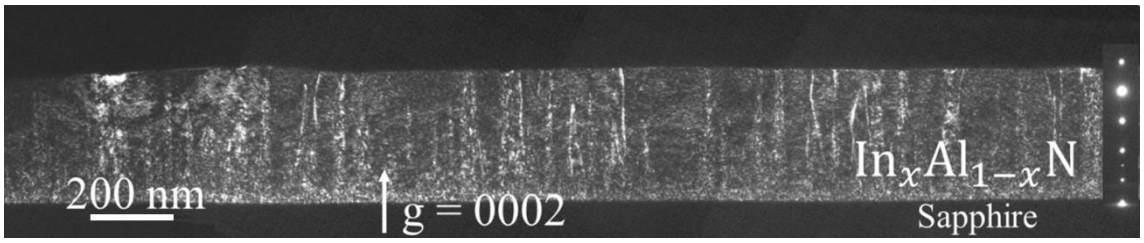

Figure 6. Weak beam dark field cross sectional TEM image of $In_xAl_{1-x}N$ on sapphire: **g** = 0002.

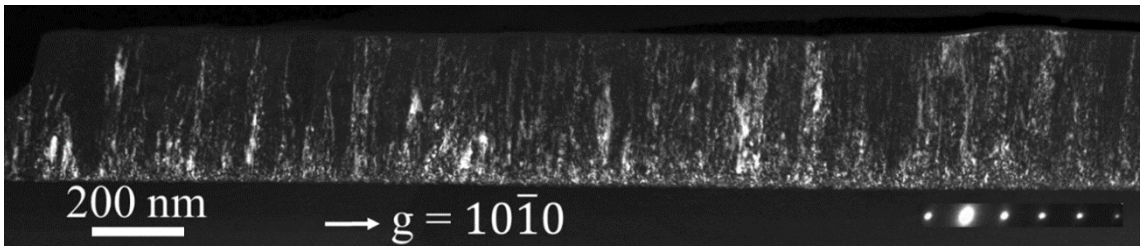

Figure 7. Weak beam dark field cross sectional TEM image of $In_xAl_{1-x}N$ on sapphire: **g** = $10\bar{1}0$.

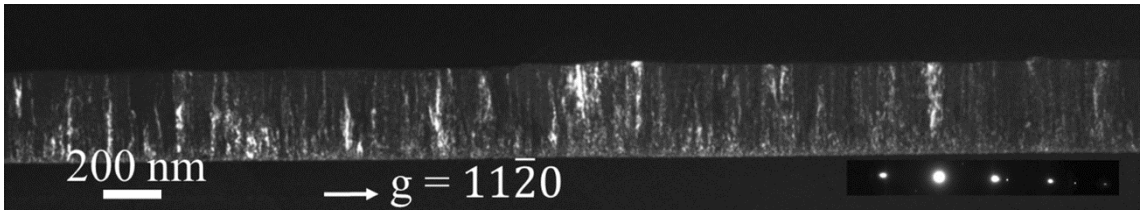

Figure 8. Weak beam dark field cross sectional TEM image of $In_xAl_{1-x}N$ on sapphire: **g** = $11\bar{2}0$.

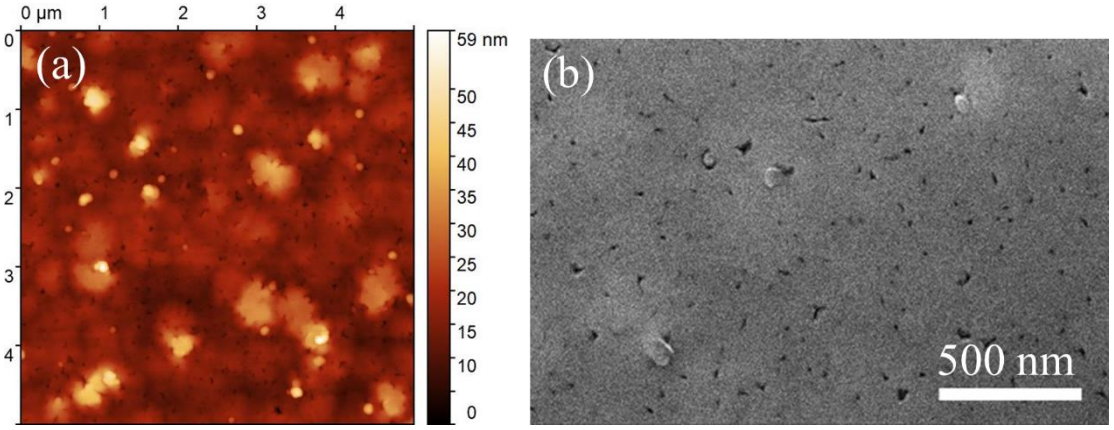

Figure 9. (a) AFM and (b) SEM images of the surface of $In_xAl_{1-x}N$ layer on sapphire.

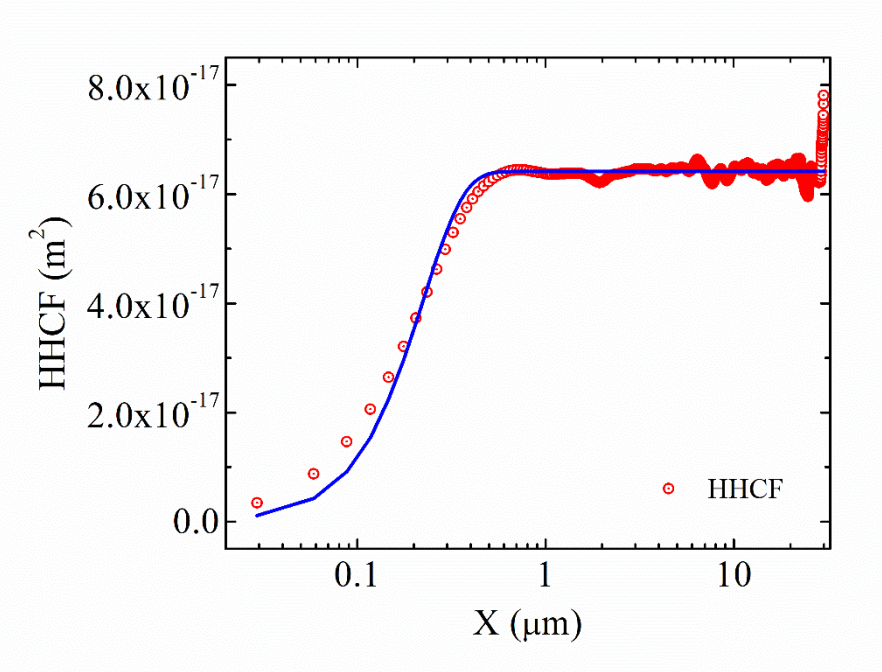

Figure 10. HHCF variation with one of the spatial coordinate X for $In_xAl_{1-x}N$ layer on sapphire. Solid blue line shows the fitting of the overall experimental data (red open circles).

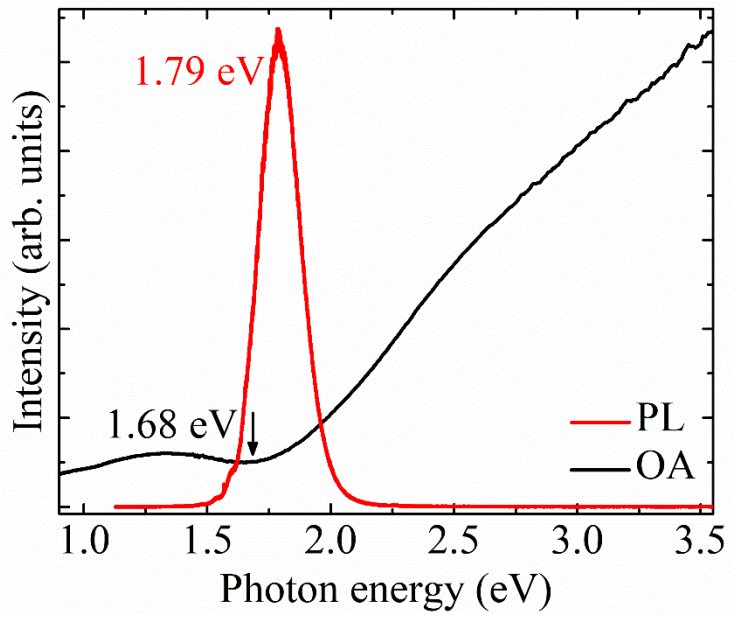

Figure 11. Room temperature optical spectra of $In_{0.60}Al_{0.40}N$ layer measured by different techniques: (a) optical-absorbance (OA); and (b) photoluminescence (PL).

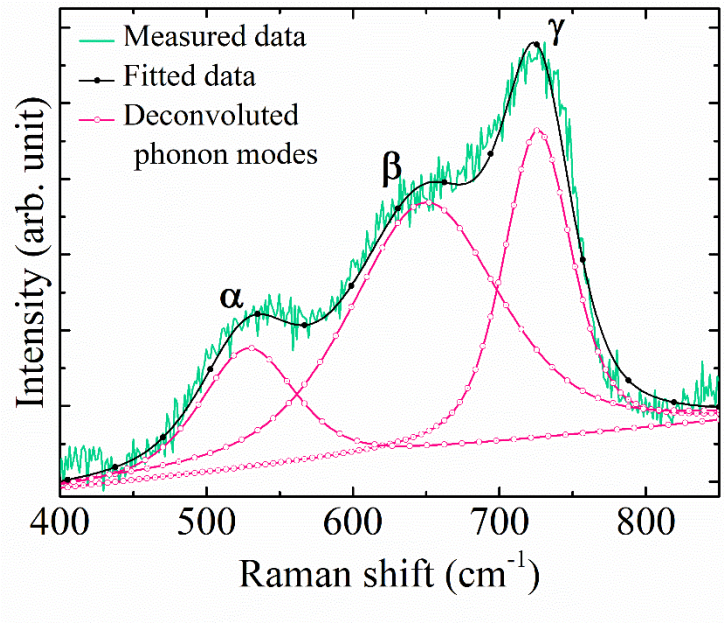

Figure 12. Room-temperature Raman spectra of $In_{0.60}Al_{0.40}N$ layer obtained in $z(xx)\bar{z}$ geometry. α, β and γ consecutively denote E_2(high), InN-like A_1(LO) and AlN-like A_1(LO) phonon modes.

References

[1] V. Y. Davydov, A. A. Klochikhin, V. V. Emtsev, D. A. Kurdyukov, S. V. Ivanov, V. A. Vekshin, F. Bechstedt, J. Furthmüller, J. Aderhold, J. Graul, A. V. Mudryi, H. Harima, A. Hashimoto, A. Yamamoto, and E. E. Haller, Band gap of hexagonal InN and InGaN alloys, Phys. Status Solidi B 234 (3) (2002) 787-795.

[2] P. Lu, R. Collazo, R.F. Dalmau, G. Durkaya, N. Dietz, B. Raghothamachar, M. Dudley, Z. Sitar: Seeded growth of AlN bulk crystals in m- and c-orientation, J. Cryst. Growth 312 (1) (2009) 58.

[3] H. Angerer, D. Brunner, F. Freudenberg, O. Ambacher, and M. Stutzmann, R. Höpler, T. Metzger, and E. Born, G. Dollinger, A. Bergmaier, S. Karsch, and H.-J. Körner, Determination of the Al mole fraction and the band gap bowing of epitaxial $Al_xGa_{1-x}N$ films, Appl. Phys. Lett. 71 (1997) 1504.

[4] C. Stampfl and C. Van de Walle, Density-functional calculations for III–V nitrides using the local density approximation and the generalized gradient approximation, Phys. Rev. B 59 (8) (1999) 5521.

[5] W. Paszkowicz, R. Cerny, and S. Krukowski, Rietveld refinement for indium nitride in the 105–295 K range, Powder Diffr. 18 (2003) 114.

[6] N. Sarazin, E. Morvan, M. A. di Forte Poisson, M. Oualli, C. Gaquière, O. Jardel, O. Drisse, M. Tordjman, M. Magis, and S. L. Delage, AlInN/AlN/GaN HEMT Technology on SiC with 10W-mm and 50% PAE at 10GHz, IEEE Elec. Dev. Lett. 31 (1) (5337923) (2010) 11-13.

[7] C. Durand, J. F. Carlin, C. Bougerol, B. Gayral, D. Salomon, J. P. Barnes, J. Eymery, R. Butte, and N. Grandjean, Thin-wall GaN/InAlN multiple quantum well tubes, Nano Lett. 17 (6) (2017) 3347–3355.

[8] R. Butté, J. F. Carlin, E Feltin, M. Gonschorek, S. Nicolay, G. Christmann, D. Simeonov, A. Castiglia, J Dorsaz, H. J. Buehlmann, S. Christopoulos, G. Baldassarri Höger von Högersthal, A. J. D. Grundy, M. Mosca, C. Pinquier, M. A. Py, F. Demangeot, J. Frandon, P. G. Lagoudakis, J. J. Baumberg, and N. Grandjean, Current status of AlInN layer lattice matched to GaN for photonic & electronic, J Phys. D: Appl. Phys. 40 (2007) 6328-6344.

[9] J. F. Carlin and M. Ilegems, High-quality AlInN for high index contrast Bragg mirrors lattice matched to GaN, Appl. Phys. Lett. 83 (2003) 668.

[10] A. Castiglia, D. Simeonov, H. J. Bühlmann, J.-F. Carlin, E. Feltin, J. Dorsaz, R. Butté, and N. Grandjean, Efficient current injection scheme for nitride vertical cavity surface emitting lasers, Appl. Phys. Lett. 90 (2007) 033514.

[11] J. Kuzmík and A. Georgakilas, Proposal of high-electron mobility transistors with strained InN channel, IEEE Transactions on Electron Devices 58 (2011) 3.

[12] Q. Y. Wei, T. Li, Y. Huang, J. Y. Huang, Z. T. Chen, T. Egawa, and F. A. Ponce, Compositional instability in InAlN/GaN lattice-matched epitaxy, Appl. Phys. Lett. 100 (2012) 092101.

[13] G. P. Merceroz, G. Cosendey, J. F. Carlin, R. Butté, and N. Grandjean, Intrinsic degradation mechanism of nearly lattice-matched InAlN layers grown on GaN Substrates, J. Appl. Phys. 113 (2013) 063506.

[14] K. Starosta, RF sputtering of $Al_xIn_{1-x}N$ thin films, Phys. Status Solidi A 68 (1981) K55.

[15] Q. Guo, T. Tanaka, M. Nishio, and H. Ogawa, Optical Bandgap Energy of Wurtzite In-Rich AlInN Alloys, Jpn. J. Appl. Phys. 42 (2003) L141-L143.

[16] J. Wu, W. Walukiewicz, K. M. Yu, J. W. Ager III, S. X. Li, E. E. Haller, Hai Lu, and William J. Schaff, Universal bandgap bowing in group-III nitride alloys, Solid State Communications 127 (2003) 411–414.

[17] W. Terashima, S. B. Che, Y. Ishitani, and A. Yoshikawa, Growth and Characterization of AlInN Ternary Alloys in Whole Composition Range and Fabrication of InN/AlInN Multiple Quantum Wells by RF Molecular Beam Epitaxy, Jpn. J. Appl. Phys. 45 (2006) L539.

[18] R. E. Jones, R. Broesler, K. M. Yu, J. W. Ager III, E. E. Haller, W. Walukiewicz, X. Chen, W. J. Schaff, Band gap bowing parameter of $In_xAl_{1-x}N$, J. Appl. Phys. 104 (2008) 123501.

[19] C. Hums, J. Bläsing, A. Dadgar, A. Diez, T. Hempel, J. Christen, A. Krost, K. Lorenz, E. Alves, Metal-organic vapor phase epitaxy and properties of AlInN in the whole compositional Range, Appl. Phys. Lett. 90 (2007) 022105.

[20] T. T. Kang, A. Hashimoto, and A. Yamamoto, Raman scattering of indium-rich AlInN: Unexpected two-mode behavior of A1(LO), Phys. Rev. B 79 (2009) 033301.

[21] K. Wang, R. W. Martin, D. Amabile, P. R. Edwards, S. Hernandez, E. Nogales, K. P. O'Donnell, K. Lorenz, E. Alves, V. Matias, A. Vantomme, D. Wolverson, and I. M. Watson, Optical energies of AlInN layers, J. Appl. Phys. 103 (2008) 073510.

[22] H. Ben Ammar, A. Minj, P. Gamarra, C. Lacam, M. Tordjman, M. A. di Forte-Poisson, M. P. Chauvat, and P. Ruterana, Gallium incorporation in InAlN: role of

the chamber design and history, and the effects of growth pressure, Phys. Status Solidi A 214 (4) (2017) 1600441.

[23] Q. Guo, T. Tanaka, M. Nishio, and H. Ogawa, Structural and Optical Properties of AlInN Films Grown on Sapphire Substrates, Jpn. J. Appl. Phys. 47 (2008) 612.

[24] L. F. Jiang, W. Z. Shen, and Q. X. Guo, Temperature dependence of the optical properties of AlInN, J. Appl. Phys. 106 (2009) 013515.

[25] L. F. Jiang, J. F. Kong, W. Z. Shen, and Q. X. Guo, Temperature dependence of Raman scattering in AlInN, J. Appl. Phys. 109 (2011) 113514.

[26] A. F. Wright, Elastic properties of zinc-blende and wurtzite AlN, GaN, and InN, J. Appl. Phys. 82 (1997) 2833.

[27] P. Chauhan, S. Hasenöhrl, E. Dobročka, Ľ. Vančo, R. Stoklas, J. Kováč, P. Šiffalovič, and J. Kuzmík, Effect of temperature and carrier gas on the properties of thick $In_xAl_{1-x}N$ layer, Appl. Surf. Sci. 470 (2019) 1.

[28] C. S. Gallinat, G. Koblmüller, Feng Wu, and J. S. Speck, Evaluation of threading dislocation densities in In- and N-face InN, J. Appl. Phys. 107 (2010) 053517.

[29] H. Naoi, K. Fujiwara, S. Takado, M. Kurouchi, D. Muto, T. Araki, H. Na, and Y. Nanishi, Growth of In-Rich $In_xAl_{1-x}N$ Films on (0001) Sapphire by RF-MBE and their Properties, J. Electron. Mater. 36 (10) (2007) 1313.

[30] S. S. Kushvaha, M. Senthil Kumar, K. K. Maurya, M. K. Dalai, and N. D. Sharma, Highly c-axis oriented growth of GaN film on sapphire (0001) by laser molecular beam epitaxy using HVPE grown GaN bulk target, AIP Adv. 3 (2013) 092109.

[31] R Collazo, S. Mita, R. Schlesser and Z. Sitar, Polarity control of GaN thin films grown by metalorganic vapor phase epitaxy, Phys. Status Solidi C 2 (7) (2005) 2117.

[32] S. Mohn, N. Stolyarchuk, T. Markurt, R. Kirste, M. P. Hoffmann, R. Collazo, A. Courville, R. D. Felice, and Z. Sitar, Polarity Control in Group-III Nitrides beyond Pragmatism, Phys. Rev. Applied 5 (2016) 054004.

[33] N. Stolyarchuk, T. Markurt, A. Courville, K. March, O. Tottereau, P. Vennéguès, and M. Albrecht, Impact of sapphire nitridation on formation of Al-polar inversion domains in N-polar AlN epitaxial layers, J. Appl. Phys. 122 (2017) 155303.

[34] Galina Popovici, Wook Kim, Andrei Botchkarev, Haipeng Tang, Hadis Morkoç, and James Solomon, Impurity contamination of GaN epitaxial films from the sapphire, SiC and ZnO substrates, Appl. Phys. Lett. 71 (1997) 3385.

[35] J. Sumner, S. Das Bakshi, R. A. Oliver, M. J. Kappers, and C. J. Humphreys, Unintentional doping in GaN assessed by scanning capacitance microscopy, phys. stat. sol. (b) 245 (5) (2008) 896.

[36] J. J. Zhu, Y. M. Fan, H. Zhang, G. J. Lu, H. Wang, D. G. Zhao, D. S. Jiang, Z. S. Liu, S. M. Zhang, G. F. Chen, B. S. Zhang, and H. Yang, Contribution of GaN template to the unexpected Ga atoms incorporated into AlInN epilayers grown under an indium-very-rich condition by MOCVD, J. Cryst. Growth 348 (2012) 25.

[37] M. D. Smith, E. Taylor, T. C. Sadler, V. Z. Zubialevich, K. Lorenz, H. N. Li, J. O'Connell, E. Alves, J. D. Holmes, R. W. Martin and P. J. Parbrook, Determination of Ga auto-incorporation in nominal InAlN epilayers grown by MOCVD, J. Mater. Chem. C 2 (2014) 5787.

[38] K. Lorenz, N. Franco, E. Alves, S. Pereira, I. M. Watson, R. W. Martin, and K. P. O'Donnell, Relaxation of compressively strained AlInN on GaN, J. Cryst. Growth 310 (2008) 4058.

[39] Y. Huang, A. Melton, B. Jampana, M. Jamil, J. H. Ryou, R. D. Dupuis, and I. T. Ferguson, Compositional instability in strained InGaN epitaxial layers induced by kinetic effects, J. Appl. Phys. 110(6) (2011) 064908.

[40] S. Pereira, M. R. Correia, E. Pereira, K. P. O'Donnell, C. T. Cowan, F. Sweeney, and E. Alves, Compositional pulling effects in $In_xGa_{1-x}N$/GaN layers: A combined depth-resolved cathodoluminescence and Rutherford backscattering/ channeling study, Phys. Rev. B 64 (2001) 205311.

[41] Matteo Bosi and Roberto Fornari, A study of Indium incorporation efficiency in InGaN grown by MOVPE, J. Cryst Growth 265 (2004) 434.

[42] David F. Brown, Stacia Keller, Thomas E. Mates, James S. Speck, Steven P. DenBaars, and Umesh K. Mishra, Growth and characterization of In-polar and N-polar InAlN by metal organic chemical vapor deposition, J. Appl. Phys. 107 (2010) 033509.

[43] S. Keller, N. A. Fichtenbaum, M. Furukawa, J. S. Speck, S. P. DenBaars, and U. K. Mishra, Growth and characterization of N-polar InGaN/GaN multiquantum wells, Appl. Phys. Lett. 90 (2007) 191908.

[44] Stanislav Hasenöhrl, Prerna Chauhan, Edmund Dobročka, Roman Stoklas, Ľubomír Vančo, Marián Veselý, Farah Bouazzaoui, Marie-Pierre Chauvat, Pierre Ruterana, and Ján Kuzmík, Generation of hole gas in non-inverted InAl(Ga)N/GaN heterostructures, Applied Physics Express 12 (2019) 014001.

[45] V. Potin, P. Vermaut, P. Ruterana and G. Nouet, Extended defects in wurtzite nitride semiconductors, J. Electronic Materials 27 (1998) 266.

[46] V. Potin, P. Ruterana, G. Nouet, HREM study of stacking faults in GaN layers grown on sapphire substrate, J. Phys.: Condens. Matter 12 (2000) 10301.

[47] P. Ruterana, B. Barbaray, A. Béré, P. Vermaut, A. Hairie, E. Paumier, and G. Nouet, A. Salvador, A. Botchkarev, and H. Morkoc, Formation and stability of the {11-20} stacking fault in wurtzite nitride semiconductors, Phys. Rev. B 59 (1999) 15917.

[48] X. J. Ning, F. R. Chien, and P. Pirouz, Growth defects in GaN films on sapphire: The probable origin of threading dislocations, J. Mater. Res. 11 (1996) 580.

[49] P. Ruterana, V. Potin, B. Barbaray, and G. Nouet, Growth defects in GaN layers on top of (0001) sapphire: a geometrical analysis of the misfit effect, Phil. Mag. A 80 (2000) 937.

[50] V. Narayanan, K. Lorenz, Wook Kim, and S. Mahajan, Origins of threading dislocations in GaN epitaxial layers grown on sapphire by metalorganic chemical vapor deposition, Appl. Phys. Lett. 78 (2001) 1544.

[51] P. Khomninou, T. Kehagias, G. Nouet, P. Ruterana, and T. Karakostas, Misfit Relaxation of the GaN/Al_2O_3 (0001) interface, Phys. Rev. B 64 (2001) 195329.

[52] X. H. Wu, L. M. Brown, D. Kapolnek, S. Keller, B. Keller, S. P. DenBaars, and J. S. Speck, Defect structure of metal-organic chemical vapor deposition-grown epitaxial (0001) GaN/Al_2O_3, J. Appl. Phys.80 (1996) 3228.

[53] V. Potin, G. Nouet, and P. Ruterana, The {10-10} inversion domains in GaN layers grown on (0001) sapphire: A Transmission Electron Microscopy study of the atomic structure of the boundaries, Phil. Mag. A79 (1999) 2899.

[54] P. Chauhan, S. Hasenöhrl, M. P. Chauvat, A. Minj, P. Ruterana, and J. Kuzmík, (unpublished).

[55] E. Dimakis, E. Iliopoulos, K. Tsagaraki, and A. Georgakilas, Physical model of InN growth on Ga-face GaN (0001) by molecular-beam epitaxy, Appl. Phys. Lett. 86 (2005) 133104.

[56] X. Wang, S. B. Che, Y. Ishitani, and A. Yoshikawa, Effect of epitaxial temperature on N-polar InN films grown by molecular beam epitaxy, J. Appl. Phys. 99 (2006) 073512.

[57] David Nečas, and Petr Klapetek, Gwyddion: an open-source software for SPM data analysis, Cent. Eur. J. Phys. 10(1) (2012) 181-188.

[58] Y. B. Kwon, J. H. Je, P. Ruterana, and G. Nouet, On the origin of a-type threading dislocations in GaN layers, J. Vac. Sci. Technol. A 23 (2005) 1588.

[59] S. Yamaguchi, M. Kariya, S. Nitta, T. Takeuchi, C. Wetzel, H. Amano and I. Akasaki, Anomalous features in the optical properties of InAlN on GaN grown by MOVPE, Appl. Phys. Lett. 76 (2000) 876.

[60] T. T. Kang, M. Yamamoto, M. Tanaka, A. Hashimoto, and A. Yamamoto, Effect of gas flow on the growth of In-rich AlInN films by metal-organic chemical vapor deposition, J. Appl. Phys. 106 (2009) 053525.

[61] M. Tangi, P. Mishra, B. Janjua, T. K. Ng, D. H. Anjum, A. Prabaswara, Y. Yang, A. M. Albadri, A. Y. Alyamani, M. M. El-Desouki, and B. S. Ooi, Bandgap measurements and the peculiar splitting of E_2^H phonon modes of $In_xAl_{1-x}N$ nanowires grown by plasma assisted molecular beam epitaxy, J. Appl. Phys. 120 (2016) 045701.

[62] V. Yu. Davydov, I. N. Goncharuk, A. N. Smirnov, A. E. Nikolaev, W. V. Lundin, A. S. Usikov, A. A. Klochikhin, J. Aderhold, J. Graul, and O. Semchinova, Composition dependence of optical phonon energies and Raman line broadening in hexagonal $Al_xGa_{1-x}N$ alloys, Phys. Rev. B 65 (2002) 125203.

[63] L. Bergman, M. D. Bremser, W. G. Perry, R. F. Davis, M. Dutta, and R. J. Nemanich, Raman analysis of the configurational disorder in $Al_xGa_{1-x}N$ films, Appl. Phys. Lett. 71 (1997) 2157.

[64] T. Kozawa, T. Kachi, H. Kano, Y. Taga, M. Hashimoto, N. Koide, and K. Manabe, Raman scattering from LO phononplasmon coupled modes in gallium nitride, J. Appl. Phys. 75 (1994) 1098.

[65] K. R. Bagnall, C. E. Dreyer, D. Vanderbilt, and E. N. Wang, Electric field dependence of optical phonon frequencies in wurtzite GaN observed in GaN high electron mobility transistors, J. Appl. Phys. 120 (2016) 155104.

[66] R. Oliva, J. Ibáñez, R. Cuscó, R. Kudrawiec, J. Serafinczuk, O. Martínez, J. Jiménez, M. Henini, C. Boney, A. Bensaoula, and L. Artús, Raman scattering by the E_{2h} and A_1(LO) phonons of InGaN epilayers (0.25 < x < 0.75) grown by molecular beam epitaxy, J Appl. Phys. 111 (2012) 063502.